Suppression of far-field blooming in high-power broad-area diode lasers by optimizing gain distribution

Tao Wang (王 涛)[1,2], Lijie Wang (汪丽杰)[1], Shili Shu (舒世立)[1], Sicong Tian (田思聪)[1], Zhide Zhao (赵智德)[3], Cunzhu Tong (佟存柱)[1,*], and Lijun Wang (王立军)[1]

[1]*State Key laboratory of Luminescence and Applications, Changchun Institute of Optics, Fine Mechanics and Physics, Chinese Academy of Sciences, Changchun 130033, China*

[2]*University of Chinese Academy of Sciences, Beijing 100049, China*

[3]*Suzhou Everbright Photonics Co., Ltd, Suzhou 215000, China*

**Corresponding author: tongcz@ciomp.ac.cn*

Received February 27, 2017; accepted April 7, 2017; posted online April 20, 2017

Far-field blooming, a serious far-field dependence on driving current, affects the stability of beam quality and applications of broad-area (BA) diode lasers. In this Letter, the lateral ridge waveguide (LRW) is introduced to BA lasers by a simple and cost-effective approach to control the far-field stability and beam divergence. The influences of LRW length on output power, near- and far-field, are investigated and it is found that the optimized LRW length is able to improve both the far-field blooming and output power. The mechanism behind this is analyzed and a 0.13°/A dependence of lateral divergence angle on the injection current is achieved.

OCIS codes: 140.014, 140.2020, 250.5960.
doi: 10.3788/COL201715.071404.

High-power diode lasers with broad-area (BA) waveguides are widely used for pumping of solid-state lasers and fiber lasers, direct material processing, security, and defense. However, the BA diode lasers suffer from a serious current-dependent far field (FF) in the slow axis (lateral direction of the waveguide), i.e., the FF blooming effect[1,2], which reduces significantly the brightness of diode lasers with the increase in injected current, although the power is still increasing. The injection-sensitive FF will affect the effective collimating, fiber coupling efficiency, power stability as pumping source, and so on, which limits the realistic applications of BA diode lasers.

To solve this issue, many approaches have been proposed, including external cavity techniques[3–7], thermal path engineering[8,9], and phase structures[10–12]. These methods are effective in suppressing the FF blooming effect, but increase the complexity and hence the fabrication cost, which is sensitive for the industrial manufacturing of high-power BA diode lasers. The other extensively used method is the distributed electrode design to tailor the gain distribution[13–19], which is realized by the patterned electrode, including the nonuniform electrode patterns[13–15] and multi-stripe[16–19] patterns. Although the nonuniform electrode pattern realizes the narrow slow axis FF[14,15], there is no demonstration of the improvement of FF blooming. For the multi-stripe gain devices, periodic gain profiles are formed to reduce the filamentation effect. However, the use of selective ion implantation results in the large lateral divergence[16,19] and the double-lobed FF[17,18] due to the deep modulation on the gain distribution. The restricted FF blooming effect[19] was demonstrated but with a widened lateral divergence. A simple, effective, and low cost approach is desired.

In this Letter, multiple lateral ridge waveguides (LRWs) were introduced to BA diode lasers by dry etching to manipulate the gain distribution, and the manipulation intensity was controlled by the length of the LRW. Compared to the ion implantation method, the LRW defined by the standard lithography and etching technique is easy to use to control the gain guiding accurately without the implant-generated point defects. The modified gain distribution suppresses the lateral carrier accumulation (LCA) near the edge of the mesa and the carrier dissipation in the central area. The influences of the LRW length on the near field (NF), FF pattern, as well as the output power of the BA lasers, were investigated in detail and the mechanism behind them was analyzed.

The schematic diagram of the BA LRW laser is shown in Fig. 1. The epitaxial layers were grown on n+ GaAs substrate by metal organic chemical vapor deposition (MOCVD), which is the super large optical cavity (SLOC)

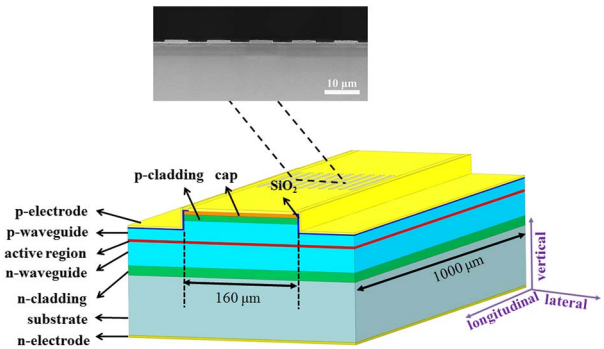

Fig. 1. Schematic diagram of the BA LRW laser under investigation.

structure[20]. The gain medium is two InGaAs/GaAsP quantum wells (QWs) and embedded in the 3.0 and 1.2 μm thick n- and p-type $Al_{0.1}Ga_{0.9}As$ layers. The emission wavelength of QWs is 965 nm. The bottom and top cladding layers are, respectively, n- and p-doped $Al_{0.15}Ga_{0.85}As$ and $Al_{0.2}Ga_{0.8}As$. The top layer is 200 nm p+ GaAs for ohmic contact.

A 160 μm wide stripe was defined by lithography and an inductively coupled plasma (ICP) etching and the etching depth was 1 μm. Then the negative photoresist was used to pattern the LRW on the mesa with an individual ridge width of 8 μm and a period of 15 μm. To realize a gain modulation on the active region, the grooves of 650 nm depth were formed through ICP etching down to a 100 nm residual p-doped cladding layer. After that, 200 nm SiO_2 was deposited and the contact window was opened with a residual of 7.5 μm SiO_2 near both sides of the mesa. Then the p-side metal contact, wafer thinning, polishing, and n-side metal contact were performed by standard processing. For experimental characterization, the single device was mounted with the p-side down on a C-mount heatsink without a facet coating. The same BA laser without LRW was fabricated from the same wafer for comparison.

Figure 2 shows the continuous-wave (CW) light power from both facets versus current (*L-I*) characteristics of the standard BA lasers and BA LRW lasers with different lengths of LRW at 20°C. The cavity length is $L = 1$ mm. Here, a ratio r of the LRW length along the longitudinal direction to the whole cavity length is defined to describe the modulation intensity of the LRW on BA lasers. $r = 10\%$ stands for the LRW length of 100 μm. Similarly, the standard BA laser is expressed as $r = 0\%$. The threshold currents of the LRW BA lasers are increased gradually with the increase of the LRW length. However, the slope efficiency increases first, and then decreases compared to the standard BA lasers. Meanwhile, the lasers with $r = 10\%$ and $r = 20\%$ have a higher output power (~4.8% and 3% at 4 A) than that of standard lasers. The improved efficiency might be due to the following reasons. The slope efficiency η_s is proportional to the internal quantum efficiency η_{in}, i.e., $\eta_s \propto \eta_{in}\alpha_m/g_{th}$. Here, α_m is the mirror loss and g_{th} is the threshold modal gain. The introduction of LRW will suppress the lateral current spreading and leaking, and hence improve the internal quantum efficiency η_{in}[21]. However, the increase of the LRW length or the ratio r will lead to a strong gain perturbation and high selfheating, and hence increase the threshold modal gain and reduce the slope efficiency. Hence, the dependence of quantum efficiency on the ratio r is intrinsic to the trade-off between the improved internal quantum efficiency and the deteriorated threshold modal gain and selfheating.

The SLOC structure diminishes the facet load and narrows the vertical FF divergence. The measured full width at half-maximum (FWHM) divergence of vertical FF is 14.2° and the divergence with a 95% power content ($\vartheta_{\perp,95\%}$) is only 26.8°. The lateral CW FF profiles at 20°C were also measured and shown. Figure 3 shows the comparison between the standard laser and LRW laser with $r = 20\%$ and $r = 100\%$. It is obvious that the laser with $r = 20\%$ has a narrower FF profile than that of the standard laser and the LRW laser with $r = 100\%$. The lateral divergence $\vartheta_{//,95\%}$ is about 8.51° at 4 A for the LRW laser with $r = 20\%$, which is decreased about 21.8% and 25.9% compared to the standard laser and LRW laser with $r = 100\%$ respectively. In addition, the LRW laser shows more peaks in the FF profile, which might be from the effect of LRW in the resonant direction.

Figure 4 shows the dependence of lateral FF divergence defined by 95% power content for standard laser and

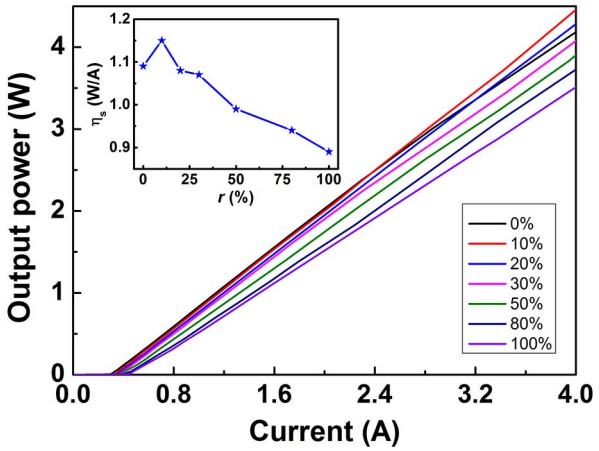

Fig. 2. Output power curves as a function of current for BA LRW lasers. The inset shows the influence of r on the slope efficiencies.

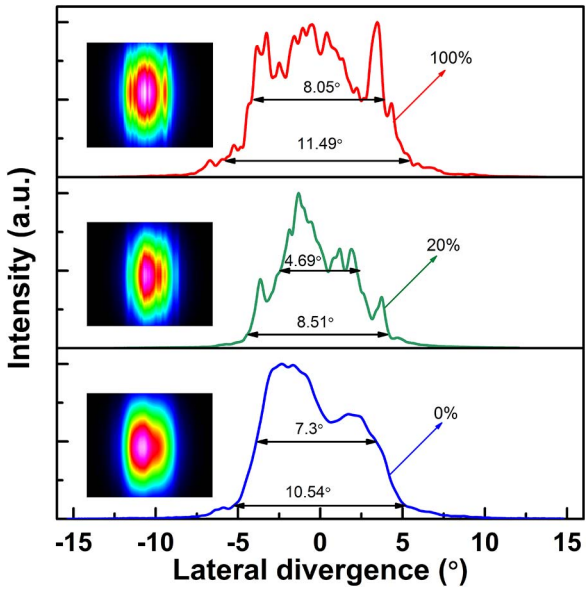

Fig. 3. Lateral FF distributions of standard laser and LRW lasers with $r = 20\%$ and $r = 100\%$ at a 4 A injection current. The insert is the real spot size, respectively.

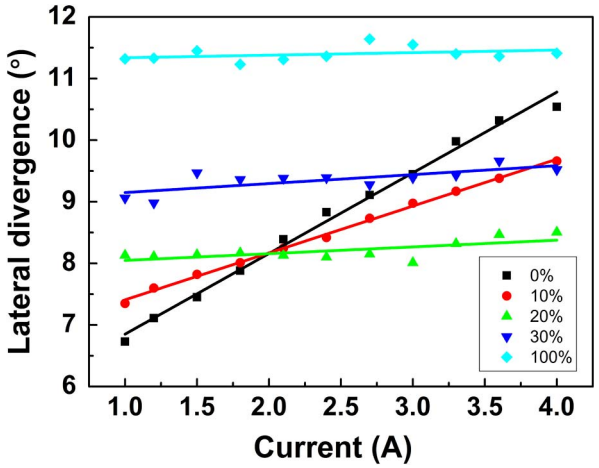

Fig. 4. Lateral divergence with 95% power content as a function of injection current.

LRW lasers. For the laser without LRW, the lateral divergence increases by 3.81° from 1 to 4 A injection current. The rapidly increased divergence indicates the serious FF blooming effect in the lateral direction. When the LRW is introduced, the FF blooming effect is evidently suppressed. The dependence of the lateral FF divergence on the injection goes down to 0.13°/A for $r = 20\%$; in contrast, it is 1.27°/A for the standard device. Continuing to increase the ratio r, the FF blooming is suppressed but with degraded lateral FF angles. The lateral divergence is over 11° for $r = 100\%$. By comparing the lateral divergence, it is found that the $r = 20\%$ is the best structure in which a good balance between the stable lateral FF and lower divergence is achieved.

To analyze the mechanism behind the lateral FF, the NF distributions were measured with a CCD camera with a 20× microscope objective. The NF characteristics of the standard laser and LRW lasers are shown in Fig. 5(a) for 1 A injection current and Fig. 5(b) for 4 A injection current. For simplification, only $r = 0\%$, 20%, and 100% are shown for comparison. A comparative analysis of these NF profiles is performed, which shows that the NF of the standard laser shows more light at the edge of the device, which reflects the more serious LCA. The LCA effect is one of the main reasons for FF blooming[22]. With the increase of r, the LCA effect is evidently suppressed, which leads to the improved injection dependence of FF. However, more peaks appear in the NF profiles that become sharper and more fluctuated. This is corresponding to the increased FF divergence when r is high, as shown in Fig. 4. Obviously, the longer the LRW, the stronger the gain modulation in the devices. Hence, too strong modulation causes a side effect on the FF angle. Similar results can be found in the previous works on tailoring the gain distribution by the ion implantation method[16–19]. The ion implantation method often leads to a strong modulation of the gain distribution and hence the large lateral divergence[16–19]. As shown in Fig. 5(a), the space of adjacent peaks is 15 μm, which is consistent with

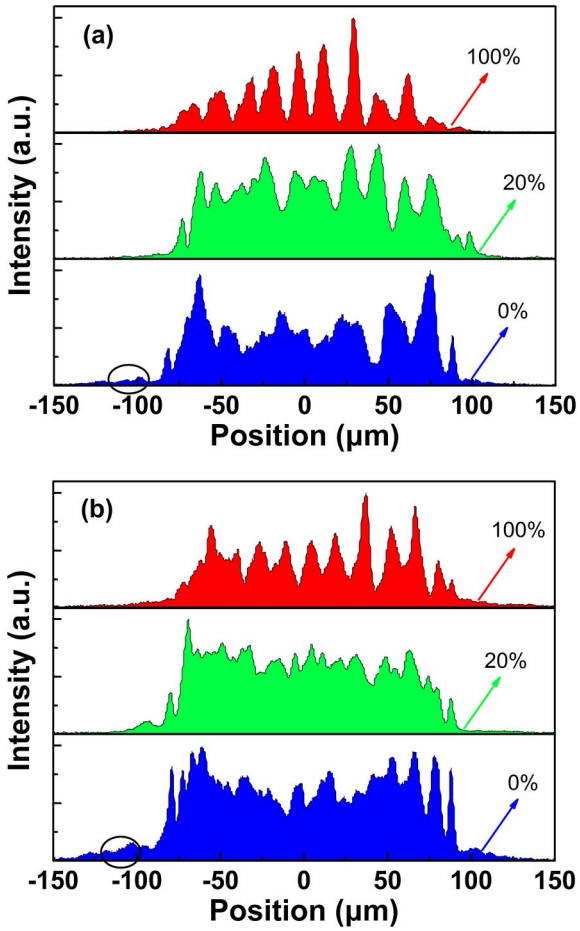

Fig. 5. Lateral NF distributions of standard laser ($r = 0\%$) and LRW lasers with $r = 20\%$ and 100% at injection currents of (a) $I = 1$ A and (b) $I = 4$ A.

the period of the LRW. When the current increases to 4 A, the intensity of the leaked light at the edge of the stripe intensifies for $r = 0\%$, and the laser with $r = 20\%$ exhibits a relatively stable NF intensity profile with small fluctuations, which is able to be concluded as the NF characteristics corresponding to low and stable lateral FF.

In conclusion, we demonstrate the capabilities of LRW for the effective suppressing of FF blooming in BA diode lasers. The influences of LRW on the quantum efficiency, output power, NF, and FF are studied. The best overall performance is obtained from the BA laser with the LRW length of 20% the cavity length. Limiting the lateral beam divergence rise to approximately 0.13° per ampere of current increase, compared to 1.27°/A for the BA diode laser, is achieved. It is demonstrated that the LRW's function on the suppression of FF blooming is due to the improvement of LCA, and longer LRW will lead to strong NF modulation and hence worsen the lateral divergence. In addition, the approach to defining the LRW via standard lithography and etching techniques is suitable for industrial manufacturing. We believe that our results will contribute to the development of high-brightness BA diode lasers.

This work was supported by the National Natural Science Foundation of China (Nos. 61404138 and 61474119), the National Basic Research Program of China (No. 2013CB933303), the International Science Technology Cooperation Program of China (No. 2013DFR00730), and the Opened Fund of the State Key Laboratory on Integrated Optoelectronics (No. IOSKL2016KF15).

References

1. A. Bawamia, B. Eppich, K. Paschke, H. Wenzel, F. Schnieder, G. Erbert, and G. Tränkle, Appl. Phys. B **97**, 95 (2009).
2. P. Crump, S. Böldicke, C. Schultz, H. Ekhteraei, H. Wenzel, and G. Erbert, Semicond. Sci. Technol. **27**, 045001 (2012).
3. N. Stelmakh, Proc. SPIE **7230**, 72301B (2009).
4. M. Niebuhr, C. Zink, A. Jechow, A. Heuer, L. B. Glebov, and R. Menzel, Opt. Express **23**, 12394 (2015).
5. J. Ge, J. Chen, A. Hermerschmidt, and H. Eichler, Chin. Opt. Lett. **1**, 334 (2003).
6. W. Huang, X. Zeng, and Y. An, Chin. Opt. Lett. **1**, 475 (2003).
7. D. Lu, K. Huang, F. Wang, and D. Yang, Chin. Opt. Lett. **1**, 656 (2003).
8. J. G. Bai, P. Leisher, S. Zhang, S. Elim, M. Grimshaw, C. Bai, L. Bintz, D. Dawson, L. Bao, and J. Wang, Proc. SPIE **7953**, 79531F (2011).
9. J. Piprek, IEEE Photon. Technol. Lett. **25**, 958 (2013).
10. H. C. Eckstein, U. D. Zeitner, K. Ahmed, W. Schmid, and U. Strauss, Proc. SPIE **7953**, 79531J (2011).
11. H. C. Eckstein, U. D. Zeitner, A. Tünnermann, W. Schmid, U. Strauss, and C. Lauer, Opt. Lett. **38**, 4480 (2013).
12. H. C. Eckstein, U. D. Zeitner, A. Tünnermann, C. Lauer, and U. Strauss, Proc. SPIE **9382**, 93821H (2015).
13. P. Salet, F. Gerard, T. Fillion, A. Pinquier, J. L. Gentner, S. Delepine, and P. Doussiere, IEEE Photon. Technol. Lett. **10**, 1706 (1998).
14. B. X. Bo, X. Gao, L. Wang, H. Li, and Y. Qu, IEEE Photon. Technol. Lett. **16**, 1248 (2004).
15. C. Lindsey, P. Derry, and A. Yariv, Electron. Lett. **21**, 671 (1985).
16. M. V. Maximov, Y. M. Shernyakov, I. I. Novikov, L. Y. Karachinsky, N. Y. Gordeev, U. Ben-Ami, D. Bortman-Arbiv, A. Sharon, V. A. Shchukin, and N. N. Ledentsov, IEEE J. Sel. Top. Quantum Electron. **14**, 1113 (2008).
17. R. Platz, G. Erbert, W. Pittroff, M. Malchus, K. Vogel, and G. Tränkle, High Power Laser Sci. Eng. **1**, 60 (2013).
18. G. Sobczak, E. Dąbrowska, M. Teodorczyk, J. Kalbarczyk, and A. Maląg, Proc. SPIE **8702**, 87020B (2013).
19. G. Sobczak, E. Dąbrowska, M. Teodorczyk, K. Krzyżak, and A. Malag, IEEE J. Quantum Electron. **50**, 890 (2014).
20. T. Wang, C. Tong, L. Wang, Y. Zeng, S. Tian, S. Shu, J. Zhang, and L. J. Wang, Appl. Phys. Express **9**, 112102 (2016).
21. C. Chen, P. Leisher, S. Patterson, P. Crump, Y. K. Kim, and K. Choquette, Appl. Phys. Lett. **94**, 011107 (2009).
22. M. Winterfeldt, P. Crump, S. Knigge, A. Maaßdorf, U. Zeimer, and G. Erbert, IEEE Photon. Technol. Lett. **27**, 1809 (2015).